Journal of Elasticity **66:** 47–62, 2002.

Bounding Envelopes in Multiphase Material Design

T.I. ZOHDI
Department of Mechanical Engineering, 6195 Etcheverry Hall, University of California, Berkeley, CA 94720-1740, USA. E-mail: zohdi@newton.berkeley.edu

Received 28 August 2001; in revised form 26 April 2002

Abstract. In practice, whenever determining macroscopic effective mechanical properties of materials possessing irregular heterogeneous microstructure, one can only test, numerically or experimentally, finite sized samples. Such materials are exemplified by randomly distributed particles suspended in a homogeneous binding matrix. If one were to compute the effective responses of various equal finite sized samples, with the only mutually distinguishing feature being the various random distributions of the particulate matter, fluctuations would occur. While such fluctuations can be small for large samples, their effects become amplified when computing design sensitivities, such as gradients and Hessians, for macroscopic effective property optimization strategies. Concisely stated, these fluctuations can severely impair the performance of such approaches by destroying the quality of the derivatives. A natural way of eliminating the negative effects of such fluctuations is by ensemble averaging the response of multiple samples until the results stabilize, and then to construct the sensitivities with the stabilized results. The focus of this work is to interpret such an ensemble regularization process, in particular when it is incorporated into effective property design procedures. It is shown that, under certain conditions, this type of regularization produces upper and lower bounding envelopes for objective functions representing desired macroscopic effective responses associated with idealized, *fluctuation free*, material samples of infinite size.

Mathematics Subject Classifications (2000): 35J20, 74E05, 74E35.

Key words: micro-heterogeneity, optimization, primal and complementary principles.

1. Introduction

Presently, a variety of new solid materials, possessing highly heterogeneous microstructure, are used in modern applications. One class of such materials consists of particles or fibers suspended in a binding matrix material (Figure 1). Mathematically, the mechanical properties of microheterogeneous materials are characterized by a spatially variable elasticity tensor $\mathbb{E} \in \mathcal{R}^{3^2\times 3^2}$ whose components satisfy, $\forall \boldsymbol{\epsilon} \in \mathcal{R}^{3\times 3}$, $\boldsymbol{\epsilon} = \boldsymbol{\epsilon}^T$, $a^-\boldsymbol{\epsilon} : \boldsymbol{\epsilon} \leqslant \boldsymbol{\epsilon} : \mathbb{E} : \boldsymbol{\epsilon} \leqslant a^+\boldsymbol{\epsilon} : \boldsymbol{\epsilon}$, $0 < a^-, a^+ < \infty$, $\forall \boldsymbol{x} \in \Omega$, where $E_{ijkl} = E_{jikl} = E_{ijlk} = E_{klij}$, $1 \leqslant i, j, k, l \leqslant 3$, and where E_{ijkl} are the Cartesian components of $\mathbb{E}$. An important research issue in the analysis and design such materials is the determination of the effective mechanical properties of the microheterogeneous material, usually characterized by a relation between

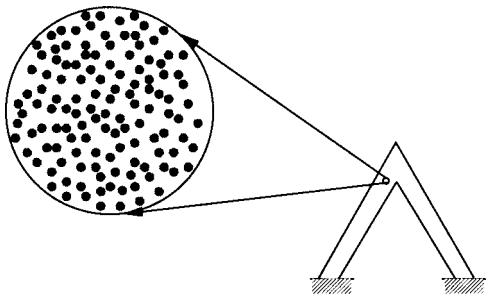

Figure 1. A solid body possessing a heterogeneous microstructure.

averages, $\mathbb{E}^*$, defined through $\langle \boldsymbol{\sigma} \rangle_\Omega = \mathbb{E}^* : \langle \boldsymbol{\epsilon} \rangle_\Omega$. Here,

$$\langle \cdot \rangle_\Omega \stackrel{\text{def}}{=} \frac{1}{|\Omega|} \int_\Omega \cdot \, \mathrm{d}\Omega,$$

and $\boldsymbol{\sigma}$ and $\boldsymbol{\epsilon}$ are the stress and strain fields within a statistically representative volume element (RVE) with volume $|\Omega|$. The reader is referred to reviews of the state of the art in the analysis of random heterogeneous media found in the recent works of Torquato [1–4].

1.1. FUNDAMENTAL DIFFICULTIES

It is clear that for the relation between averages to be useful, i.e. statistically representative, the sample must be so large that, for further enlargements, $\mathbb{E}^*$ does not change. Unfortunately, detailed boundary value representations resolving the heterogeneous microstructure require a huge numerical effort that can overwhelm even the most modern computational facilities. In short, solutions to partial differential equations posed over statistically representative samples of irregular microheterogeneous material are still open problems, *even in the case of linearized elasticity*. Therefore, due to the inability to directly simulate a statistically representative volume element, one must settle for computing responses of sub-statistically representative, finite sized, samples.

It is obvious that if the samples were infinite in size compared to the particles, there would be no fluctuations in the responses, but clearly this is impossible to test from either a computational or experimental point of view. A primary problem associated with computing macroscopic effective mechanical responses of finite sized samples of materials possessing heterogeneous irregular microstructure is that equal sized samples exhibit mutual fluctuations from one another. Therefore, when testing multiple finite sized samples, no single effective response ($\mathbb{E}^*$) will be obtained, but rather a distribution of responses ($\mathbb{E}^* \pm \Delta\mathbb{E}^*$). Detailed studies and reviews addressing size effects in effective responses of heterogeneous media can be found in [5–18]. Such fluctuations can have negative consequences when incorporated into inverse effective property design methodologies, where design

sensitivities involving derivatives must be computed. As an example, consider the construction of an inverse problem, where combinations of particulate and matrix materials are sought which minimize the following normalized objective function

$$\Pi = \left(\frac{\|\mathbb{E}^* - \mathbb{E}^{*,D}\|}{\|\mathbb{E}^{*,D}\|} \right)^2, \tag{1}$$

where $\mathbb{E}^{*,D}$ is a prespecified desired effective response, and where $\|\cdot\|$ is an appropriate norm, to be specified later in the work. A microstructural design can be defined through an N-tuple design vector, denoted $\mathbf{\Lambda} \stackrel{\text{def}}{=} (\Lambda_1, \Lambda_2, \ldots, \Lambda_N)$, for example, consisting of the following components: (1) the mechanical properties of constituents (matrix and particles), (2) the respective volume fractions, and (3) the topologies of the particles.* While fluctuations in the effective responses may be small for large samples, they are amplified when computing effective property design sensitivities, for example when forming quantities like

$$\frac{\partial \Pi(\mathbf{\Lambda})}{\partial \Lambda_i} \quad \text{and} \quad \frac{\partial^2 \Pi(\mathbf{\Lambda})}{\partial \Lambda_i \partial \Lambda_j}, \quad i, j = 1, \ldots, N,$$

where N is the number of design components. For example, such quantities are needed in Quasi-Newton optimization schemes. However, even in nonderivative objective function evaluation/comparison schemes, such as some forms of genetic algorithms, the fluctuations can force such algorithms to malfunction, or to completely break down. A natural way of eliminating the negative effects of macroscopic property fluctuations is by ensemble averaging multiple samples until the results stabilize, and to form the sensitivities with the stabilized results. It is the focus of this work to interpret such an ensemble regularization process when it is incorporated into effective property design procedures.

1.2. OBJECTIVES OF THIS WORK

The outline of the presentation is as follows. In section two, some background information on effective responses is given. In section three, the consequences of the effective property perturbations are investigated, along with an ensemble regularization technique. In section four, the process is mathematically analyzed, and the physical meaning of the results is ascertained. In section five, some concluding comments are given.

REMARK. In order to make the presentation clear, we primarily discuss materials consisting of a homogeneous base matrix with identical randomly dispersed particles, although the forthcoming analysis is relatively general and can be applied to a variety of other microstructural material types.

* Ellipsoidal shapes are qualitatively useful since the geometry can mimic a variety of microstructures, for example, platelets, when the ellipsoids are strongly oblate, or needles or chopped fibers, when the ellipsoids are strongly prolate.

2. Background Information

A sample of heterogeneous material occupying an open bounded domain in $\Omega \in \mathcal{R}^3$, under a given set of specified boundary loadings, is considered. Its boundary is denoted $\partial\Omega$. The body is in static equilibrium under the action of body forces, $\boldsymbol{f}$, and surface tractions, $\boldsymbol{t}$. The boundary $\overline{\partial\Omega} = \overline{\Gamma_u \cup \Gamma_t}$ consists of a part Γ_u and a part Γ_t on which displacements and tractions are respectively prescribed. Following standard notation, $H^1(\Omega)$ is denoted as the usual space of functions with generalized partial derivatives of order $\leqslant 1$ in $L^2(\Omega)$. The symbol $\boldsymbol{H}^1(\Omega) \stackrel{\text{def}}{=} [H^1(\Omega)]^3$ is defined as the space of vector-valued functions whose components have generalized partial derivatives $\leqslant 1$ in $\boldsymbol{L}^2(\Omega) \stackrel{\text{def}}{=} [L^2(\Omega)]^3$. The symbol "$\boldsymbol{u}|_{\partial\Omega}$" is used for generalized boundary values, for example for specified boundary displacements. Throughout the analysis, the microstructure is assumed to be perfectly bonded. A general variational boundary value representation is

$$\boxed{\begin{array}{l}\text{Find } \boldsymbol{u} \in \boldsymbol{H}^1(\Omega),\ \boldsymbol{u}|_{\Gamma_u} = \boldsymbol{d}, \quad \text{such that} \\ \\ \displaystyle\int_\Omega \nabla \boldsymbol{v} : \mathbb{E} : \nabla \boldsymbol{u}\, \mathrm{d}\Omega = \int_\Omega \boldsymbol{f} \cdot \boldsymbol{v}\, \mathrm{d}\Omega + \int_{\Gamma_t} \boldsymbol{t} \cdot \boldsymbol{v}\, \mathrm{d}A, \quad \forall \boldsymbol{v} \in \boldsymbol{H}^1(\Omega), \quad \boldsymbol{v}|_{\Gamma_u} = \boldsymbol{0}.\end{array}} \tag{2}$$

The data are assumed to be such that $\boldsymbol{f} \in \boldsymbol{L}^2(\Omega)$ and $\boldsymbol{t} \in \boldsymbol{L}^2(\Gamma_t)$, but less smooth data can be considered without complications. It is convenient to consider the sample domain (Ω) as a cube, although, strictly speaking, this is not necessary. A commonly accepted macro/micro criterion used in effective property calculations is the well-known Hill condition, $\langle \boldsymbol{\sigma} : \boldsymbol{\epsilon} \rangle_\Omega = \langle \boldsymbol{\sigma} \rangle_\Omega : \langle \boldsymbol{\epsilon} \rangle_\Omega$. Hill's condition dictates the size requirements on the sample to be statistically representative. The classical argument is as follows. For any perfectly bonded heterogeneous body, in the absence of body forces ($\boldsymbol{f} = \boldsymbol{0}$), two physically relevant loading states satisfy Hill's condition. They are (1) pure linear boundary displacements of the form $\boldsymbol{u}|_{\partial\Omega} = \mathcal{E} \cdot \boldsymbol{x}$, which implies $\langle \boldsymbol{\epsilon} \rangle_\Omega = \mathcal{E}$ and (2) pure boundary tractions in the form $\boldsymbol{t}|_{\partial\Omega} = \mathcal{L} \cdot \boldsymbol{n}$, which implies $\langle \boldsymbol{\sigma} \rangle_\Omega = \mathcal{L}$, where $\mathcal{E}$ and $\mathcal{L}$ are constant strain and stress tensors, respectively. Clearly, for Hill's condition to be satisfied within a macroscopic body under nonuniform external loading, the sample must be large enough to possess small boundary field fluctuations relative to its size. Therefore applying type (1) or (2) boundary conditions to a large sample is a way of reproducing approximately what may be occurring in a statistically representative mesoscopic subdomain of material within a macroscopic body.⋆ Explicitly, to determine $\mathbb{E}^*$, one specifies six linearly independent loadings of the form, (1) $\boldsymbol{u}|_{\partial\Omega} = \mathcal{E}^{(I \to VI)} \cdot \boldsymbol{x}$ or (2) $\boldsymbol{t}|_{\partial\Omega} = \mathcal{L}^{(I \to VI)} \cdot \boldsymbol{n}$, where $\mathcal{E}^{(I \to VI)}$ and $\mathcal{L}^{(I \to VI)}$

⋆ If the sample were infinite in size in comparison to the length scales of the microstructure, and $\mathcal{L} = \mathbb{E}^* : \mathcal{E}$, then these test loading would be identical.

are symmetric second order strain and stress tensors, with spatially constant components. Each independent loading state provides six equations, for a total of 36 (15 of which are redundant), which are used to determine the 21 components of the tensor relation between average stress and strain, $\mathbb{E}^*$. If the effective response is assumed isotropic then only one test loading (instead of usually six), possessing nonzero dilatational ($(tr\boldsymbol{\sigma})/3$ and $(tr\boldsymbol{\epsilon})/3$) and deviatoric components ($\boldsymbol{\sigma}'$ and $\boldsymbol{\epsilon}'$), is necessary to determine the effective bulk and shear moduli.

3. Effective Property Design/Multi-Microvariable Searches

We consider the following natural objective function for effective property design:

$$\Pi = \left(\frac{\mathcal{E} : (\mathbb{E}^* - \mathbb{E}^{*,D}) : \mathcal{E}}{\mathcal{E} : \mathbb{E}^{*,D} : \mathcal{E}} \right)^2. \tag{3}$$

When considering an effective material design process, the boundary value problem in box (2) has to be solved, depending on the degree of anisotropy, possibly up to six times, for each new microstructure ($\mathbb{E}$), in order to generate $\mathbb{E}^*$. Following a standard Newton-type multivariate search, a new design increment, $\Delta\boldsymbol{\Lambda} \stackrel{\text{def}}{=} (\Delta\Lambda_1, \Delta\Lambda_2, \ldots, \Delta\Lambda_N)$, for a microstructural design vector, $\boldsymbol{\Lambda}$, is achieved by solving the following system, $[\mathbb{H}]\{\Delta\boldsymbol{\Lambda}\} = -\{\boldsymbol{g}\}$, where $[\mathbb{H}]$ is the Hessian matrix $(N \times N)$, with components $H_{ij} = \partial^2\Pi(\boldsymbol{\Lambda})/(\partial\Lambda_i\partial\Lambda_j)$, $\{\boldsymbol{g}\}$ is the gradient $(N \times 1)$, with components $g_i = \partial\Pi(\boldsymbol{\Lambda})/\partial\Lambda_i$ and where $\{\Delta\boldsymbol{\Lambda}\}$ is the design increment $(N \times 1)$, with components $\Delta\Lambda_i$. After the design increment has been solved for, one then forms an updated design vector, $\boldsymbol{\Lambda}^{\text{new}} = \boldsymbol{\Lambda}^{\text{old}} + \Delta\boldsymbol{\Lambda}$, and the process is repeated until $\|\Pi\| \leqslant TOL$.

3.1. NUMERICAL DIFFERENTIATION

As with most complicated systems, finite difference approximations of the gradient and Hessian components are constructed with respect to the design parameters. The finite difference size for the approximate numerical derivatives, which is different for each component, is denoted h_{Λ_i}. In a practical setting, for example, for each variable, the numerical derivative step sizes are scaled to the size of the current value of that variable, by a small number $0 < \theta \ll 1$, $\theta \times \boldsymbol{\Lambda}_i = h_{\Lambda_i}$. Numerically, the components of the gradient are approximated by the following second order central finite difference stencils:

$$\begin{aligned} \frac{\partial\Pi(\boldsymbol{\Lambda})}{\partial\Lambda_i} \approx & \frac{\Pi(\Lambda_1, \Lambda_2, \ldots, \Lambda_i + h_{\Lambda_i}, \ldots, \Lambda_N)}{2h_{\Lambda_i}} \\ & - \frac{\Pi(\Lambda_1, \Lambda_2, \ldots, \Lambda_i - h_{\Lambda_i}, \ldots, \Lambda_N)}{2h_{\Lambda_i}}, \end{aligned} \tag{4}$$

while for the components of the Hessian we have

$$\frac{\partial^2 \Pi(\mathbf{\Lambda})}{\partial \Lambda_i^2} \approx \frac{\Pi(\Lambda_1, \Lambda_2, \ldots, \Lambda_i + h_{\Lambda_i}, \ldots, \Lambda_N) - 2\Pi(\Lambda_1, \Lambda_2, \ldots, \Lambda_i, \ldots, \Lambda_N)}{h_{\Lambda_i}^2} + \frac{\Pi(\Lambda_1, \Lambda_2, \ldots, \Lambda_i - h_{\Lambda_i}, \ldots, \Lambda_N)}{h_{\Lambda_i}^2} \tag{5}$$

and

$$\begin{aligned}\frac{\partial^2 \Pi(\mathbf{\Lambda})}{\partial \Lambda_i \partial \Lambda_j} \approx & \frac{\Pi(\Lambda_1, \Lambda_2, \ldots, \Lambda_i + h_{\Lambda_i}, \ldots, \Lambda_j + h_{\Lambda_j}, \ldots, \Lambda_N)}{4h_{\Lambda_i} h_{\Lambda_j}} \\ & + \frac{\Pi(\Lambda_1, \Lambda_2, \ldots, \Lambda_i - h_{\Lambda_i}, \ldots, \Lambda_j - h_{\Lambda_j}, \ldots, \Lambda_N)}{4h_{\Lambda_i} h_{\Lambda_j}} \\ & - \left(\frac{\Pi(\Lambda_1, \Lambda_2, \ldots, \Lambda_i - h_{\Lambda_i}, \ldots, \Lambda_j + h_{\Lambda_j}, \ldots, \Lambda_N)}{4h_{\Lambda_i} h_{\Lambda_j}} \right. \\ & \left. + \frac{\Pi(\Lambda_1, \Lambda_2, \ldots, \Lambda_i + h_{\Lambda_i}, \ldots, \Lambda_j - h_{\Lambda_j}, \ldots, \Lambda_N)}{4h_{\Lambda_i} h_{\Lambda_j}} \right).\end{aligned} \tag{6}$$

The number of objective function evaluations necessary to form the Hessian and gradient is $2N^2 + 1$, where N is the number of microstructural design variables. This stems from the fact that one needs $2(N^2 - N)$ objective evaluations for the off-diagonal terms of the Hessian, $2N$ for the diagonal terms, and one evaluation for the base point (the current design). Therefore even with a small number of design variables the number of objective function evaluations can be quite large. For example, with only four variables, (1) the bulk modulus of the particulate additives, (2) the shear modulus of the particulate additives, (3) the volume fraction of the particulate additives, and (4) the aspect ratio of the particulate additives (assuming ellipsoids), one has $2N^2 + 1 = 2(16) + 1 = 33$ objective function evaluations per search step. It is clear that the construction of the discrete Hessian is the main expense. There exist a variety of quasi-Newton methods, which in some manner attempt to approximate the Hessian in an inexpensive way (see [19]). However, regardless of the reduction of the number costly objective function evaluations, such procedures require an immense amount of effort which grows dramatically with sample size.

3.2. A NATURAL ENSEMBLE REGULARIZATION

Referring to Figure 2, during the construction of numerical derivatives, the effects of fluctuations due sample size can be characterized by computing the highest value on the left, and lowest value on the right, resulting in

$$\delta^+ = \frac{(\mathbb{E}^*(\mathbf{\Lambda} + \Delta\mathbf{\Lambda}) + \Delta\mathbb{E}^*_+(\mathbf{\Lambda} + \Delta\mathbf{\Lambda})) - (\mathbb{E}^*(\mathbf{\Lambda} - \Delta\mathbf{\Lambda}) - \Delta\mathbb{E}^*_-(\mathbf{\Lambda} - \Delta\mathbf{\Lambda}))}{\|\mathbb{E}^*(\mathbf{\Lambda} + \Delta\mathbf{\Lambda}) - \mathbb{E}^*(\mathbf{\Lambda} - \Delta\mathbf{\Lambda})\|}, \tag{7}$$

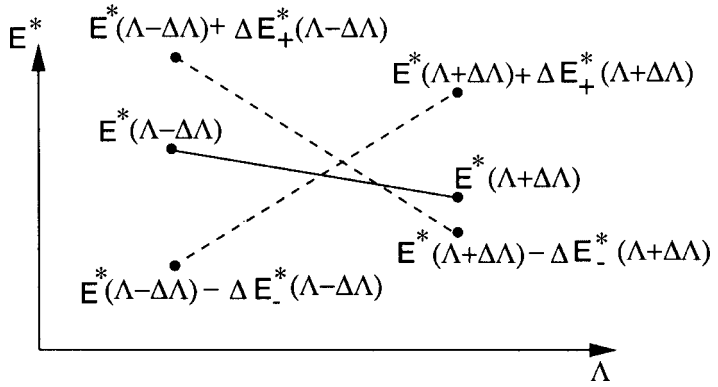

Figure 2. Perturbations in the computation of a numerical derivative.

and computing the lowest value on the left, and highest value on the right, resulting in

$$\delta^- = \frac{(\mathbb{E}^*(\mathbf{\Lambda} + \Delta\mathbf{\Lambda}) - \Delta\mathbb{E}^*_-(\mathbf{\Lambda} + \Delta\mathbf{\Lambda})) - (\mathbb{E}^*(\mathbf{\Lambda} - \Delta\mathbf{\Lambda}) + \Delta\mathbb{E}^*_+(\mathbf{\Lambda} - \Delta\mathbf{\Lambda}))}{\|\mathbb{E}^*(\mathbf{\Lambda} + \Delta\mathbf{\Lambda}) - \mathbb{E}^*(\mathbf{\Lambda} - \Delta\mathbf{\Lambda})\|}, \tag{8}$$

and taking their difference

$$\|\delta^+ - \delta^-\| = \frac{\|\Delta\mathbb{E}^*_+(\mathbf{\Lambda} + \Delta\mathbf{\Lambda}) + \Delta\mathbb{E}^*_-(\mathbf{\Lambda} + \Delta\mathbf{\Lambda}) + \Delta\mathbb{E}^*_+(\mathbf{\Lambda} - \Delta\mathbf{\Lambda}) + \Delta\mathbb{E}^*_-(\mathbf{\Lambda} - \Delta\mathbf{\Lambda})\|}{\|\mathbb{E}^*(\mathbf{\Lambda} + \Delta\mathbf{\Lambda}) - \mathbb{E}^*(\mathbf{\Lambda} - \Delta\mathbf{\Lambda})\|}. \tag{9}$$

Clearly, the effects of the fluctuations are amplified during numerical differentiation. Therefore, even for large samples of randomly dispersed particulate material, which may exhibit slight fluctuations from one another, the resulting deviations in derivatives can be quite large. A natural stabilization procedure is to test multiple sample of the same size (for a given $\mathbf{\Lambda}$) and then to ensemble average the results. Specifically, consider a certain microstructural design specification ($\mathbf{\Lambda}$), and a process where a sample of finite size, with a random microstructure, is tested, and the effective response recorded. Consider a repetition of the test for another equal sized sample, with the same microstructural design vector, however with another random microstructural realization. The tests are repeated, for more and more samples, until the sequential change in the ensemble average falls below a given tolerance for further tests ($i = 1, 2, \ldots, S$)

$$\left| \frac{1}{S+1} \sum_{i=1}^{S+1} \Pi^{(i)} - \frac{1}{S} \sum_{i=1}^{S} \Pi^{(i)} \right| \leqslant TOL \left| \frac{1}{S+1} \sum_{i=1}^{S+1} \Pi^{(i)} \right|. \tag{10}$$

The ensemble averaging procedure can be incorporated into a Newton type optimization scheme by

(1) computing, for multiple samples, each component needed for the construction of the gradient and Hessian $\boldsymbol{\Lambda} \pm h_{\Lambda_i}$, until the ensemble average for each stabilizes,
(2) post-processing the ensemble averaged components to form

$$\frac{\partial \Pi(\boldsymbol{\Lambda})}{\partial \Lambda_i}, \frac{\partial^2 \Pi(\boldsymbol{\Lambda})}{\partial \Lambda_i \partial \Lambda_j}, \quad i, j = 1, \ldots, N,$$

(3) solving the Hessian system, $[\mathbb{H}]\{\Delta \boldsymbol{\Lambda}\} = -\{\boldsymbol{g}\}$, for the design vector increment $\Delta \boldsymbol{\Lambda}$ and
(4) repeating the process until the potential is below a certain tolerance $\|\Pi\| \leqslant TOL$.

A fundamental issue is to ascertain what is actually being minimized by such a natural ensemble averaging optimization process. This is discussed next.

REMARK 1. From a practical point of view, adaptively selecting the number of samples needed to stabilize the results is important since (1) it is impossible to know a priori how many samples to test for the ensemble average to stabilize and (2) it more cost effective than simply taking a large (overkill) preset number of samples.

REMARK 2. Even alternative approaches to Quasi-Newton methods such as Genetic Algorithms based upon rapid, non-derivative objective function evaluation will also suffer from effective property fluctuations due to the inability to accurately compare neighboring objective function values for various designs. For reviews of such methods, the interested reader is referred to [20–22]. A recent overview of the state of the art of the field can be found in a collection of recent articles, edited by Goldberg and Deb [23].

4. Ensemble Averaging Interpretation via Minimum Principles

In order to analyze size effects we employ a type of domain decomposition.

4.1. A PRIMAL DECOMPOSITION

Consider a (large) sample of material with the following general boundary value representation

Find $\boldsymbol{u} \in \boldsymbol{H}^1(\Omega)$, $\boldsymbol{u}|_{\Gamma_u} = \boldsymbol{d}$, such that

$$\int_\Omega \nabla \boldsymbol{v} : \underbrace{\mathbb{E} : \nabla \boldsymbol{u}}_{\boldsymbol{\sigma}} \, \mathrm{d}\Omega = \int_\Omega \boldsymbol{f} \cdot \boldsymbol{v} \, \mathrm{d}\Omega + \int_{\Gamma_t} \boldsymbol{t} \cdot \boldsymbol{v} \, \mathrm{d}A, \quad \forall \boldsymbol{v} \in \boldsymbol{H}^1(\Omega), \quad \boldsymbol{v}|_{\Gamma_u} = \boldsymbol{0}. \tag{11}$$

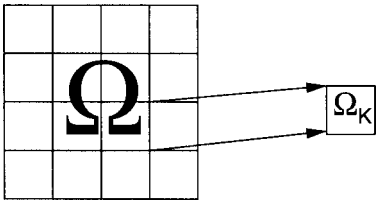

Figure 3. A cross-section of a domain decomposition of a sample of material. Only for pictorial convenience are the sample and subsamples shown to be rectangular.

Now partition the domain into S subdomains, $\Omega = \cup_{K=1}^{S} \Omega_K$. The pieces do not have to be the same size or shape, although for illustration purposes it is convenient to take a uniform (regular) partitioning (Figure 3). Consider a kinematically admissible function, $\boldsymbol{U} \in \boldsymbol{H}^1(\Omega)$ and $\boldsymbol{U}|_{\Gamma_u} = \boldsymbol{d}$, which is projected onto the *internal boundaries* ($\partial\Omega_K$) of the subdomains. Any subdomain boundaries coinciding with the exterior surface retain their original boundary conditions (Figure 3). Accordingly, we have the following virtual work formulation, for each subdomain, $1 \leqslant K \leqslant S$:

$$\begin{aligned}
&\text{Find } \tilde{\boldsymbol{u}}_K \in \boldsymbol{H}^1(\Omega_K), \quad \tilde{\boldsymbol{u}}_K|_{\partial\Omega_K \cap (\Omega \cup \Gamma_u)} = \boldsymbol{U} \in \boldsymbol{H}^1(\Omega), \quad \text{such that} \\
&\int_{\Omega_K} \nabla \boldsymbol{v}_K : \underbrace{\mathbb{E} : \nabla \tilde{\boldsymbol{u}}_K}_{\tilde{\boldsymbol{\sigma}}_K} \, \mathrm{d}\Omega = \int_{\Omega_K} \boldsymbol{f} \cdot \boldsymbol{v}_K \, \mathrm{d}\Omega + \int_{\partial\Omega_K \cap \Gamma_t} \boldsymbol{t} \cdot \boldsymbol{v}_K \, \mathrm{d}A \\
&\forall \boldsymbol{v}_K \in \boldsymbol{H}^1(\Omega_K), \quad \boldsymbol{v}_K|_{\partial\Omega_K \cap (\Omega \cup \Gamma_u)} = \boldsymbol{0}.
\end{aligned} \tag{12}$$

The individual subdomain solutions, $\tilde{\boldsymbol{u}}_K$, are zero outside of the corresponding subdomain $\overline{\Omega}_K$. In this case the approximate solution is constructed by a direct assembly process, $\tilde{\boldsymbol{u}} \overset{\text{def}}{=} \boldsymbol{U} + (\tilde{\boldsymbol{u}}_1 - \boldsymbol{U})|_{\Omega_1} + (\tilde{\boldsymbol{u}}_2 - \boldsymbol{U})|_{\Omega_2} + \cdots + (\tilde{\boldsymbol{u}}_S - \boldsymbol{U})|_{\Omega_S}$. The approximate displacement field is in $\boldsymbol{H}^1(\Omega)$, however, the approximate traction field is possibly discontinuous. Logical choices of $\boldsymbol{U}$, i.e. $\boldsymbol{U} = \mathcal{E} \cdot \boldsymbol{x}$, will be given momentarily. It should be clear that if $\boldsymbol{U} = \boldsymbol{u}$ on the internal partition boundaries, then the approximate solution is exact. Since we employ energy type variational principles to generate approximate solutions, we use an induced energy norm to measure the solution differences

$$0 \leqslant \|\boldsymbol{u} - \tilde{\boldsymbol{u}}\|^2_{E(\Omega)} \overset{\text{def}}{=} \int_{\Omega} \nabla(\boldsymbol{u} - \tilde{\boldsymbol{u}}) : \mathbb{E} : \nabla(\boldsymbol{u} - \tilde{\boldsymbol{u}}) \, \mathrm{d}\Omega. \tag{13}$$

It is convenient to cast the error in terms of the potential energy,

$$\mathcal{J}(\boldsymbol{w}) \overset{\text{def}}{=} \frac{1}{2} \int_{\Omega} \nabla \boldsymbol{w} : \mathbb{E} : \nabla \boldsymbol{w} \, \mathrm{d}\Omega - \int_{\Omega} \boldsymbol{f} \cdot \boldsymbol{w} \, \mathrm{d}\Omega - \int_{\Gamma_t} \boldsymbol{t} \cdot \boldsymbol{w} \, \mathrm{d}A,$$

where $\boldsymbol{w}$ is any kinematically admissible function. This leads to $\|\boldsymbol{u} - \boldsymbol{w}\|^2_{E(\Omega)} = 2(\mathcal{J}(\boldsymbol{w}) - \mathcal{J}(\boldsymbol{u}))$ or $\mathcal{J}(\boldsymbol{u}) \leqslant \mathcal{J}(\boldsymbol{w})$, which is a form of the Principle of Minimum

Potential Energy. In other words, the true solution possesses a minimum potential. By direct substitution we have

$$0 \leqslant \|\boldsymbol{u} - \tilde{\boldsymbol{u}}\|^2_{E(\Omega)} = 2\big(\mathcal{J}(\tilde{\boldsymbol{u}}) - \mathcal{J}(\boldsymbol{u})\big). \tag{14}$$

In the special case that $\boldsymbol{u}|_{\partial\Omega} = \mathcal{E} \cdot \boldsymbol{x}$, which is equivalent to testing each subsample with $\boldsymbol{u}|_{\partial\Omega_K} = \mathcal{E} \cdot \boldsymbol{x}$, equation (14) imples

$$\boxed{0 \leqslant \|\boldsymbol{u} - \tilde{\boldsymbol{u}}\|^2_{E(\Omega)} = \mathcal{E} : \big(\widetilde{\mathbb{E}}^* - \mathbb{E}^*\big) : \mathcal{E}|\Omega|,} \tag{15}$$

where $\langle\tilde{\boldsymbol{\sigma}}\rangle_{\Omega_K} \stackrel{\text{def}}{=} \widetilde{\mathbb{E}}^*_K : \langle\tilde{\boldsymbol{\epsilon}}\rangle_{\Omega_K}$ and $\widetilde{\mathbb{E}}^* \stackrel{\text{def}}{=} \sum_{K=1}^{S} \widetilde{\mathbb{E}}^*_K(|\Omega_K|/|\Omega|)$.

4.2. A COMPLEMENTARY DECOMPOSITION

We can repeat the partitioning process for an applied internal traction set of tests. The equivalent complementary form for the exact (undecomposed) problem is

$$\boxed{\begin{aligned}&\text{Find } \boldsymbol{\sigma}, \quad \nabla \cdot \boldsymbol{\sigma} + \boldsymbol{f} = \boldsymbol{0}, \quad \boldsymbol{\sigma} \cdot \boldsymbol{n}|_{\Gamma_t} = \boldsymbol{t} \quad \text{such that}\\ &\int_\Omega \boldsymbol{\tau} : \mathbb{E}^{-1} : \boldsymbol{\sigma}\, \mathrm{d}\Omega = \int_{\Gamma_u} \boldsymbol{\tau} \cdot \boldsymbol{n} \cdot \boldsymbol{d}\, \mathrm{d}A, \quad \forall \boldsymbol{\tau}, \quad \nabla \cdot \boldsymbol{\tau} = \boldsymbol{0}, \quad \boldsymbol{\tau} \cdot \boldsymbol{n}|_{\Gamma_t} = \boldsymbol{0}.\end{aligned}} \tag{16}$$

For the complementary problem, similar restrictions are placed on the solution and test fields to force the integrals to make sense. In other words, we assume that solutions produce finite global energy. When employing the applied internal traction approach, in order to construct approximate solutions, a statically admissible function, $\boldsymbol{\Sigma}$, with the property that $\boldsymbol{\Sigma} \cdot \boldsymbol{n}|_{\Gamma_t} = \boldsymbol{t}$, is projected onto the *internal boundaries* of the subdomain partitions. As in the applied displacement case, any subdomain boundaries coinciding with the exterior surface retain their original boundary conditions. Accordingly, we have the following complementary virtual work formulation, for each subdomain, $1 \leqslant K \leqslant S$:

$$\boxed{\begin{aligned}&\text{Find } \hat{\boldsymbol{\sigma}}_K, \quad \nabla \cdot \hat{\boldsymbol{\sigma}}_K + \boldsymbol{f} = \boldsymbol{0}, \quad \hat{\boldsymbol{\sigma}}_K \cdot \boldsymbol{n}|_{\partial\Omega_K \cap (\Omega \cup \Gamma_t)} = \boldsymbol{\Sigma} \cdot \boldsymbol{n}|_{\partial\Omega_K \cap (\Omega \cup \Gamma_t)}\\ &\text{such that}\\ &\int_{\Omega_K} \boldsymbol{\tau}_K : \mathbb{E}^{-1} : \hat{\boldsymbol{\sigma}}_K\, \mathrm{d}\Omega = \int_{\Gamma_u} \boldsymbol{\tau}_K \cdot \boldsymbol{n} \cdot \boldsymbol{d}\, \mathrm{d}A\\ &\forall \boldsymbol{\tau}_K, \quad \nabla \cdot \boldsymbol{\tau}_K = \boldsymbol{0}, \quad \boldsymbol{\tau}_K \cdot \boldsymbol{n}|_{\partial\Omega_K \cap (\Omega \cup \Gamma_t)} = \boldsymbol{0}.\end{aligned}} \tag{17}$$

The individual subdomain solutions, $\hat{\boldsymbol{\sigma}}_K$, are zero outside of the corresponding subdomain $\overline{\Omega}_K$. In this case the approximate solution is constructed by a direct assembly process $\hat{\boldsymbol{\sigma}} \stackrel{\text{def}}{=} \boldsymbol{\Sigma} + (\hat{\boldsymbol{\sigma}}_1 - \boldsymbol{\Sigma})|_{\Omega_1} + (\hat{\boldsymbol{\sigma}}_2 - \boldsymbol{\Sigma})|_{\Omega_2} + \cdots + (\hat{\boldsymbol{\sigma}}_S - \boldsymbol{\Sigma})|_{\Omega_S}$. The

stress field is statically admissible, however, the approximate displacement field is possibly discontinuous. Logical choices of $\boldsymbol{\Sigma}$, $\boldsymbol{\Sigma} = \mathcal{L} = \textit{constant}$, will be given momentarily. It should be clear that if $\boldsymbol{\Sigma} = \boldsymbol{\sigma}$ on the internal partition boundaries, then the approximate solution is exact. We define the complementary norm

$$0 \leqslant \|\boldsymbol{\sigma} - \hat{\boldsymbol{\sigma}}\|^2_{E^{-1}(\Omega)} \stackrel{\text{def}}{=} \int_\Omega (\boldsymbol{\sigma} - \hat{\boldsymbol{\sigma}}) : \mathbb{E}^{-1} : (\boldsymbol{\sigma} - \hat{\boldsymbol{\sigma}})\, \mathrm{d}\Omega. \tag{18}$$

As in the primal case, it is convenient to cast the error in terms of the potential complementary energy for the case of linear elasticity, where $\mathcal{K}(\boldsymbol{\gamma}) \stackrel{\text{def}}{=} \frac{1}{2}\int_\Omega \boldsymbol{\gamma} : \mathbb{E}^{-1} : \boldsymbol{\gamma}\, \mathrm{d}\Omega - \int_{\Gamma_u} \boldsymbol{\gamma} \cdot \boldsymbol{n} \cdot \boldsymbol{u}\, \mathrm{d}A$, where $\boldsymbol{\gamma}$ is any statically admissible function. The well known relationship, for a statically admissible function $\boldsymbol{\gamma}$, is $\|\boldsymbol{\sigma} - \boldsymbol{\gamma}\|^2_{E^{-1}(\Omega)} = 2(\mathcal{K}(\boldsymbol{\sigma}) - \mathcal{K}(\boldsymbol{\sigma}))$ or $\mathcal{K}(\boldsymbol{\sigma}) \leqslant \mathcal{K}(\boldsymbol{\gamma})$. This is a form of the Principle of Minimum Complementary Potential Energy. In other words, the true solution possesses a minimum complementary potential. Choosing $\boldsymbol{\gamma} = \hat{\boldsymbol{\sigma}}$, we have

$$0 \leqslant \|\boldsymbol{\sigma} - \hat{\boldsymbol{\sigma}}\|^2_{E(\Omega)} = 2\big(\mathcal{K}(\hat{\boldsymbol{\sigma}}) - \mathcal{K}(\boldsymbol{\sigma})\big). \tag{19}$$

In the special case that $\boldsymbol{t}|_{\partial\Omega} = \mathcal{L} \cdot \boldsymbol{n}$, which is equivalent to testing each subsample with $\boldsymbol{t}|_{\partial\Omega_K} = \mathcal{L} \cdot \boldsymbol{n}$, equation (19) imples

$$\boxed{0 \leqslant \|\boldsymbol{\sigma} - \hat{\boldsymbol{\sigma}}\|^2_{E^{-1}(\Omega)} = \mathcal{L} : \big(\widehat{\mathbb{E}}^{-1*} - \mathbb{E}^{-1*}\big) : \mathcal{L}|\Omega|,} \tag{20}$$

where $\langle\hat{\boldsymbol{\epsilon}}\rangle_{\Omega_K} \stackrel{\text{def}}{=} \widehat{\mathbb{E}}^{-1*}_K : \langle\hat{\boldsymbol{\sigma}}\rangle_{\Omega_K}$ and $\widehat{\mathbb{E}}^{-1*} \stackrel{\text{def}}{=} \sum_{K=1}^S \widehat{\mathbb{E}}^{-1*}_K(|\Omega_K|/|\Omega|)$.

REMARK. If the sample is statistically representative, we have $\mathbb{E}^{-1*} = \mathbb{E}^{*-1}$, then boxes (15) and (20) imply, under the assumption that the uniform loadings are arbitrary, the following two sided ordering of approximate effective material responses,

$$\boxed{\big\langle\mathbb{E}^{-1}\big\rangle^{-1}_\Omega \leqslant \big(\widehat{\mathbb{E}}^{-1*}\big)^{-1} \leqslant \mathbb{E}^* \leqslant \widetilde{\mathbb{E}}^* \leqslant \langle\mathbb{E}\rangle_\Omega,} \tag{21}$$

where the tensor inequality notation means, for example, that the difference tensor $(\widetilde{\mathbb{E}}^* - \mathbb{E}^*)$ is positive definite, etc. Since $\mathcal{J}(\tilde{\boldsymbol{u}}) \leqslant \mathcal{J}(\boldsymbol{U})$, we also have $\widetilde{\mathbb{E}}^* \leqslant \langle\mathbb{E}\rangle_\Omega$. Alternatively, since $\mathcal{K}(\hat{\boldsymbol{\sigma}}) \leqslant \mathcal{K}(\mathcal{L})$, then $\widehat{\mathbb{E}}^{-1*} \leqslant \langle\mathbb{E}^{-1}\rangle_\Omega$. To the knowledge of the author, the result in box (21) was first derived in [8], however by other analysis techniques. We note that by adding together the potential energy and the complementary energy we obtain an equation of balance:

$$\begin{aligned}\mathcal{J}(\boldsymbol{u}) + \mathcal{K}(\boldsymbol{\sigma}) = \frac{1}{2}\int_\Omega \nabla\boldsymbol{u} : \mathbb{E} : \nabla\boldsymbol{u}\, \mathrm{d}\Omega - \int_\Omega \boldsymbol{f} \cdot \boldsymbol{u}\, \mathrm{d}\Omega - \int_{\Gamma_t} \boldsymbol{t} \cdot \boldsymbol{u}\, \mathrm{d}A \\ + \frac{1}{2}\int_\Omega \boldsymbol{\sigma} : \mathbb{E}^{-1} : \boldsymbol{\sigma}\, \mathrm{d}\Omega - \int_{\Gamma_u} (\boldsymbol{\sigma} \cdot \boldsymbol{n}) \cdot \boldsymbol{d}\, \mathrm{d}A = 0.\end{aligned} \tag{22}$$

As a consequence, by adding the results in equations (14) and (19) we obtain $2(\mathcal{J}(\tilde{\boldsymbol{u}}) + \mathcal{K}(\hat{\boldsymbol{\sigma}})) = \|\boldsymbol{u} - \tilde{\boldsymbol{u}}\|^2_{E(\Omega)} + \|\boldsymbol{\sigma} - \hat{\boldsymbol{\sigma}}\|^2_{E^{-1}(\Omega)}$, since $\mathcal{J}(\boldsymbol{u}) + \mathcal{K}(\boldsymbol{\sigma}) = 0$.

This last result provides a direct way to monitor size effects during material design. In the special uniform loading case we have $2(\mathcal{J}(\tilde{\boldsymbol{u}}) + \mathcal{K}(\hat{\boldsymbol{\sigma}})) = \mathcal{E} : (\widetilde{\mathbb{E}}^* - \mathbb{E}^*) : \mathcal{E}|\Omega| + \mathcal{L} : (\widehat{\mathbb{E}}^{-1*} - \mathbb{E}^{*-1}) : \mathcal{L}|\Omega|$. This relation illustrates a "duality gap" in the effective responses which is generated by performing either traction or displacement controlled tests.

4.3. EMBEDDED ORTHOGONAL MONOTONICITIES

Since $\tilde{\boldsymbol{u}}$ is kinematically admissible, we have $\|\boldsymbol{u} - \tilde{\boldsymbol{u}}\|^2_{E(\Omega)} = 2(\mathcal{J}(\tilde{\boldsymbol{u}}) - \mathcal{J}(\boldsymbol{u}))$. If we repartition the existing subdomains into more subdomains (Figure 4), and use $\boldsymbol{U}$ for the local boundary conditions on the finer partition, upon solving the local boundary value problems and assembling the local solutions together (just as before for $\tilde{\boldsymbol{u}}$), we have, denoting the solution by $\tilde{\tilde{\boldsymbol{u}}}$, $\|\tilde{\boldsymbol{u}} - \tilde{\tilde{\boldsymbol{u}}}\|^2_{E(\Omega)} = 2(\mathcal{J}(\tilde{\tilde{\boldsymbol{u}}}) - \mathcal{J}(\tilde{\boldsymbol{u}}))$. Adding the two previous relations together yields an orthogonal decomposition

$$\boxed{\|\boldsymbol{u} - \tilde{\tilde{\boldsymbol{u}}}\|^2_{E(\Omega)} = \|\tilde{\boldsymbol{u}} - \tilde{\tilde{\boldsymbol{u}}}\|^2_{E(\Omega)} + \|\boldsymbol{u} - \tilde{\boldsymbol{u}}\|^2_{E(\Omega)}.} \tag{23}$$

This implies that the error monotonically grows for successively finer embedded partitions. Intuitively one expects this type of growth in the error, since one is projecting more inaccurate data onto the interfaces. *Simply stated, more embedded subdomains, more error. Furthermore, the relationship is monotone.* As in the displacement controlled tests, for traction controlled tests we have

$$\boxed{\|\boldsymbol{\sigma} - \hat{\tilde{\boldsymbol{\sigma}}}\|^2_{E^{-1}(\Omega)} = \|\hat{\boldsymbol{\sigma}} - \hat{\tilde{\boldsymbol{\sigma}}}\|^2_{E^{-1}(\Omega)} + \|\boldsymbol{\sigma} - \hat{\boldsymbol{\sigma}}\|^2_{E^{-1}(\Omega)}.} \tag{24}$$

In terms of effective properties, equation (23) implies

$$\mathcal{E} : \left(\widetilde{\mathbb{E}}^* - \mathbb{E}^*\right) : \mathcal{E} = \mathcal{E} : \left(\widetilde{\widetilde{\mathbb{E}}}^* - \widetilde{\mathbb{E}}^*\right) : \mathcal{E} + \mathcal{E} : \left(\widetilde{\mathbb{E}}^* - \mathbb{E}^*\right) : \mathcal{E} \tag{25}$$

and consequently

$$\boxed{\mathbb{E}^* \leqslant \widetilde{\mathbb{E}}^* \leqslant \widetilde{\widetilde{\mathbb{E}}}^* \leqslant \cdots \text{ more embedded partitions } \cdots \leqslant \langle \mathbb{E} \rangle_\Omega,} \tag{26}$$

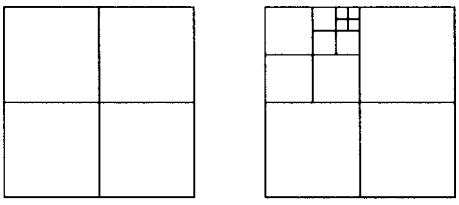

Figure 4. Embedded subdomains within subdomains.

while equation (24) implies

$$\mathcal{L} : \left(\widehat{\mathbb{E}}^{-1*} - \mathbb{E}^{-1*}\right) : \mathcal{L} = \mathcal{L} : \left(\widehat{\widehat{\mathbb{E}}}^{-1*} - \widehat{\mathbb{E}}^{-1*}\right) : \mathcal{L} + \mathcal{L} : \left(\widehat{\mathbb{E}}^{-1*} - \mathbb{E}^{-1*}\right) : \mathcal{L} \tag{27}$$

and consequently

$$\boxed{\mathbb{E}^{-1*} \leqslant \widehat{\mathbb{E}}^{-1*} \leqslant \widehat{\widehat{\mathbb{E}}}^{-1*} \leqslant \cdots \text{ more embedded partitions } \cdots \leqslant \left\langle \mathbb{E}^{-1} \right\rangle_{\Omega},} \tag{28}$$

for the traction controlled tests. The results of this section generalize and extend relations found in [8, 9, 14, 18, 24–26].

5. Primal and Dual Objective Function Envelopes and Some Concluding Remarks

Let us consider the implications of the bounds on the responses with regard to objective functions such as

$$\Pi = \left(\frac{\mathcal{E} : (\mathbb{E}^{*,D} - \mathbb{E}) : \mathcal{E}}{\mathcal{E} : \mathbb{E}^{*,D} : \mathcal{E}} \right)^2.$$

5.1. THE IMPLICATION OF $\mathbb{E}^* \leqslant \widetilde{\mathbb{E}}^*$

For illustration purposes only, consider the following scalar analogies

$$\pi\left(\widetilde{E}^*\right) = \left(\frac{E^* + \delta\widetilde{E}^* - E^{*,D}}{E^{*,D}} \right)^2 \quad \text{and} \quad \pi\left(E^*\right) = \left(\frac{E^* - E^{*,D}}{E^{*,D}} \right)^2, \tag{29}$$

where $\widetilde{E}^* = E^* + \delta\widetilde{E}^*$, $E^* > 0$, $E^{*,D} > 0$ and $\delta\widetilde{E}^* > 0$. Generally, the function $\delta\widetilde{E}^*$ varies with E^*. Referring to Figure 5, we see that if $E^* \geqslant E^{*,D}$, then $\pi(\widetilde{E}^*) \geqslant \pi(E^*)$, while if $E^* \leqslant E^{*,D} - \delta\widetilde{E}^*$, then $\pi(\widetilde{E}^*) \leqslant \pi(E^*)$. If $E^{*,D} - \delta\widetilde{E}^* \leqslant E^* \leqslant E^{*,D}$, then there is an indefinite relationship between $\pi(\widetilde{E}^*)$ and $\pi(E^*)$. For the

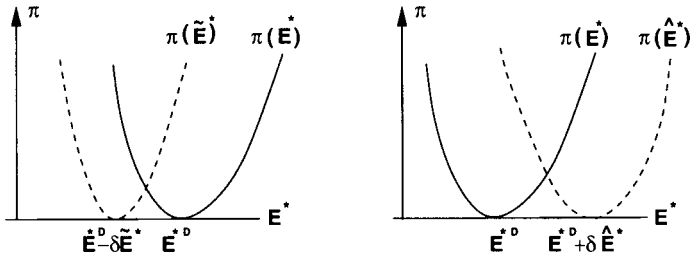

Figure 5. Upper and lower envelopes for the objective function.

tensorial analogue, the above results directly imply that, with $\widetilde{\mathbb{E}}^* = \mathbb{E}^* + \delta\widetilde{\mathbb{E}}^*$ and $\delta\widetilde{\mathbb{E}}^* \geqslant \mathbf{0}$,

$$\boxed{\begin{array}{lll} \text{IF } \mathbb{E}^* \geqslant \mathbb{E}^{*,D} & \text{THEN } \Pi\big(\widetilde{\mathbb{E}}^*\big) \geqslant \Pi(\mathbb{E}^*) & \text{(UPPER ENVELOPE),} \\ \text{IF } \mathbb{E}^* \leqslant \mathbb{E}^{*,D} - \delta\widetilde{\mathbb{E}}^* & \text{THEN } \Pi\big(\widetilde{\mathbb{E}}^*\big) \leqslant \Pi(\mathbb{E}^*) & \text{(LOWER ENVELOPE).} \end{array}} \tag{30}$$

If $\mathbb{E}^{*,D} - \delta\widetilde{\mathbb{E}}^* \leqslant \mathbb{E}^* \leqslant \mathbb{E}^{*,D}$, then there is an indefinite relationship between $\Pi(\widetilde{\mathbb{E}}^*)$ and $\Pi(\mathbb{E}^*)$.

5.2. THE IMPLICATION OF $\widehat{\mathbb{E}}^* \leqslant \mathbb{E}^*$

As in the previous subsection, following similar arguments, we have, defining $\mathbb{E}^* = \widehat{\mathbb{E}}^* + \delta\widehat{\mathbb{E}}^*$, $\delta\widehat{\mathbb{E}}^* \geqslant \mathbf{0}$,

$$\boxed{\begin{array}{lll} \text{IF } \mathbb{E}^* \geqslant \mathbb{E}^{*,D} + \delta\widehat{\mathbb{E}}^* & \text{THEN } \Pi(\widehat{\mathbb{E}}^*) \leqslant \Pi(\mathbb{E}^*) & \text{(LOWER ENVELOPE),} \\ \text{IF } \mathbb{E}^* \leqslant \mathbb{E}^{*,D} & \text{THEN } \Pi(\widehat{\mathbb{E}}^*) \geqslant \Pi(\mathbb{E}^*) & \text{(UPPER ENVELOPE).} \end{array}} \tag{31}$$

If $\mathbb{E}^{*,D} \leqslant \mathbb{E}^* \leqslant \mathbb{E}^{*,D} + \delta\widehat{\mathbb{E}}^*$, then there is an indefinite relationship between $\Pi(\widehat{\mathbb{E}}^*)$ and $\Pi(\mathbb{E}^*)$.

5.3. CLOSING COMMENTS

The preceding results imply a series of "stacked" envelopes as depicted in Figure 6, which converge to the true objective function as the sample size tends towards infinity. Furthermore, the convergence is monotone. It is clear that, in the case of displacement controlled tests, since the ensemble-generated effective responses are stiffer than the true effective response, they achieve the desired response $\mathbb{E}^{*,D}$ with microstructural designs that are, casually speaking, "softer" than the true

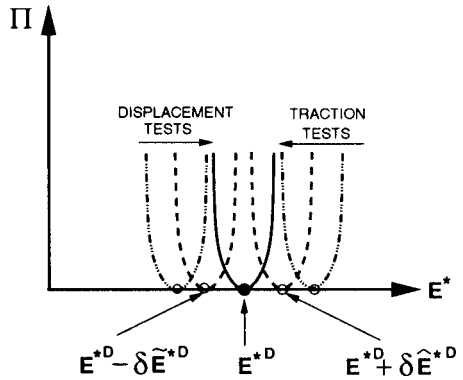

Figure 6. Two sided envelopes for the infinitely sized objective function.

minimizers. For the case of traction controlled tests, since the ensemble-generated effective responses are weaker than the true effective response, they achieve the desired response $\mathbb{E}^{*,D}$ with microstructural designs that are "harder" than the true minimizers.

Acknowledgement

The author wishes to thank Professor Christian Huet for many useful discussions.

References

1. S. Torquato, Random heterogeneous media: microstructure and improved bounds on effective properties. *Appl. Mech. Rev.* **44** (1991) 37–76.
2. S. Torquato, Effective stiffness tensor of composite media I. Exact series expansions. *J. Mech. Phys. Solids* **45** (1997) 1421–1448.
3. S. Torquato, Effective stiffness tensor of composite media II. Applications to isotropic dispersions. *J. Mech. Phys. Solids* **46** (1998) 1411–1440.
4. S. Torquato, *Random Heterogeneous Materials: Microstructure and Macroscopic Properties*. Springer, New York (2001).
5. C. Huet, Remarques sur l'assimilation d'un matériau hétérogéne á un milieu continu équivalent. In: C. Huet and A. Zaoui (eds), *Rheological Behaviour and Structure of Materials*. Presses ENPC, Paris (1981) pp. 231–245.
6. C. Huet, Universal conditions for assimilation of a heterogeneous material to an effective medium. *Mech. Res. Commun.* **9**(3) (1982) 165–170.
7. C. Huet, On the definition and experimental determination of effective constitutive equations for heterogeneous materials. *Mech. Res. Commun.* **11**(3) (1984) 195–200.
8. C. Huet, Application of variational concepts to size effects in elastic heterogeneous bodies. *J. Mech. Phys. Solids* **38** (1990) 813–841.
9. C. Huet, Hierarchies and bounds for size effects in heterogeneous bodies. In: G.A. Maugin (ed.), *Continuum Models and Discrete Systems* **2** (1991) pp. 127–134.
10. A. Guidoum and P. Navi, Numerical simulation of thermo-mechanical behaviour of concrete through a 3-D granular cohesive model. In: C. Huet (ed.), *Micromechanics of Concrete and Cementitious Composites*. Presses Polytechniques et Universitaires Romandes, Lausanne (1993) pp. 213–228.
11. M. Amieur, S. Hazanov and C. Huet, Numerical and experimental study of size and boundary conditions effects on the apparent properties of specimens not having the representative volume. In: C. Huet (ed.), *Micromechanics of Concrete and Cementitious Composite* (1993).
12. A. Guidoum, Simulation numérique 3D des comportements des bétons en tant que composites granulaires. Doctoral Dissertation No 1310, Ecole Polytechnique de Lausanne, Switzerland (1994).
13. M. Amieur, Etude numérique et expérimentale des effets d'échelle et de conditions aux limites sur des éprouvettes de béton n'ayant pas le volume représentatif. Doctoral Dissertation No 1256, Ecole Polytechnique Fédérale de Lausanne, Lausanne, Switzerland (1994).
14. S. Hazanov and C. Huet, Order relationships for boundary conditions effect in heterogeneous bodies smaller than the representative volume. *J. Mech. Phys. Solids* **42** (1994) 1995–2011.
15. S. Hazanov and M. Amieur, On overall properties of elastic heterogeneous bodies smaller than the representative volume. *Internat. J. Engrg. Sci.* **33**(9) (1995) 1289–1301.
16. M. Amieur, S. Hazanov and C. Huet, Numerical and experimental assessment of the size and boundary conditions effects for the overall properties of granular composite bodies smaller

than the representative volume. In: D.F. Parker and A.H. England (eds), *IUTAM Symposium on Anisotropy, Inhomogeneity and Nonlinearity in Solid Mechanics*. Kluwer Academic, Dordrecht (1995) pp. 149–154.
17. C. Huet, An integrated micromechanics and statistical continuum thermodynamics approach for studying the fracture behaviour of microcracked heterogeneous materials with delayed response. Special Issue of *Engineering Fracture Mechanics* **58**(5/6) (1997) 459–556.
18. C. Huet, Coupled size and boundary condition effects in viscoelastic heterogeneous bodies. *Mech. Materials* **31**(12) (1999) 787–829.
19. P. Gill, W. Murray and M. Wright, *Practical Optimization*. Academic Press, New York (1995).
20. D.E. Goldberg, *Genetic Algorithms in Search, Optimization and Machine Learning*. Addison-Wesley, Reading, MA (1989).
21. L. Davis, *Handbook of Genetic Algorithms.* Thompson Computer Press (1991).
22. C. Onwubiko, *Introduction to Engineering Design Optimization.* Prentice-Hall, Englewood Cliffs, NJ (2000).
23. D.E. Goldberg and K. Deb, Special issue on Genetic Algorithms. *Comput. Methods Appl. Mech. Engrg.* **186**(2–4) (2000) 121–124.
24. T.I. Zohdi and P. Wriggers, A domain decomposition method for bodies with microstructure based upon material regularization. *Internat. J. Solids Struct.* **36**(17) (1999) 2507–2526.
25. T. I. Zohdi, Overall solution-difference bounds on the effects of material inhomogeneities. *J. Elasticity* **58**(3) (2000) 249–255.
26. T.I. Zohdi, P. Wriggers and C. Huet, A method of substructuring large-scale computational micromechanical problems. *Comput. Methods Appl. Mech. Engrg.* **190**(43/44) (2001) 5639–5656.